

## Ground motion simulations of great earthquakes on the Alpine Fault: effect of hypocentre location and comparison with empirical modelling

Brendon A. Bradley, Sung E. Bae, Viktor Polak, Robin L. Lee, Ethan M. Thomson & Karim Tarbali

**To cite this article:** Brendon A. Bradley, Sung E. Bae, Viktor Polak, Robin L. Lee, Ethan M. Thomson & Karim Tarbali (2017) Ground motion simulations of great earthquakes on the Alpine Fault: effect of hypocentre location and comparison with empirical modelling, *New Zealand Journal of Geology and Geophysics*, 60:3, 188-198, DOI: [10.1080/00288306.2017.1297313](https://doi.org/10.1080/00288306.2017.1297313)

**To link to this article:** <https://doi.org/10.1080/00288306.2017.1297313>



Published online: 10 Apr 2017.



Submit your article to this journal 



Article views: 554



View related articles 



View Crossmark data 



Citing articles: 9 View citing articles 

RESEARCH ARTICLE



## Ground motion simulations of great earthquakes on the Alpine Fault: effect of hypocentre location and comparison with empirical modelling

Brendon A. Bradley<sup>a,b,c</sup>, Sung E. Bae<sup>b</sup>, Viktor Polak<sup>b</sup>, Robin L. Lee<sup>a</sup>, Ethan M. Thomson<sup>a</sup> and Karim Tarbali<sup>a</sup>

<sup>a</sup>Department of Civil and Natural Resources Engineering, University of Canterbury, Christchurch, New Zealand; <sup>b</sup>QuakeCoRE, University of Canterbury, Christchurch, New Zealand; <sup>c</sup>Department of Civil and Environmental Engineering, Stanford University, CA, USA

### ABSTRACT

This paper discusses simulated ground motion intensity, and its underlying modelling assumptions, for great earthquakes on the Alpine Fault. The simulations utilise the latest understanding of wave propagation physics, kinematic earthquake rupture descriptions and the three-dimensional nature of the Earth's crust in the South Island of New Zealand. The effect of hypocentre location is explicitly examined, which is found to lead to significant differences in ground motion intensities (quantified in the form of peak ground velocity, PGV) over the northern half and southwest of the South Island. Comparison with previously adopted empirical ground motion models also illustrates that the simulations, which explicitly model rupture directivity and basin-generated surface waves, lead to notably larger PGV amplitudes than the empirical predictions in the northern half of the South Island and Canterbury. The simulations performed in this paper have been adopted, as one possible ground motion prediction, in the 'Project AF8' Civil Defence Emergency Management exercise scenario. The similarity of the modelled ground motion features with those observed in recent worldwide earthquakes as well as similar simulations in other regions, and the notably higher simulated amplitudes than those from empirical predictions, may warrant a re-examination of regional impact assessments for major Alpine Fault earthquakes.

### ARTICLE HISTORY

Received 19 October 2016  
Accepted 16 February 2017

### KEYWORDS

Alpine Fault; basin-generated surface waves; directivity; emergency management; ground motion simulation

## 1. Introduction

The Alpine Fault is the major plate boundary fault in the South Island of New Zealand and accounts for 70–75% of the plate motion (Wallace et al. 2007). A significant number of studies have examined the frequency and magnitude of past large earthquakes on the Alpine Fault, with  $M_w$  8+ earthquakes expected approximately every 300–500 years (Rhoades & Van Dissen 2003; Sutherland et al. 2006; Berryman et al. 2012a, 2012b; De Pascale & Langridge 2012; Barnes et al. 2013; Ghisetti et al. 2014). The last major rupture of the Alpine Fault occurred 300 years ago in 1717 (Yetton 2000), and there is an estimated 30% probability of a major Alpine Fault rupture over the next 50 years.

Despite the understanding on Alpine fault ruptures, no previous studies have robustly examined the expected strong ground motions and ground failure for future Alpine Fault events over the South Island. Prior studies using empirical ground motion predictions (Yetton 2000; Robinson & Davies 2013) are ill-constrained for the large magnitude and source-to-site distances of interest for an Alpine Fault rupture, while high-frequency stochastic-simulation-based estimates (Holden & Zhao 2011) ignore the critically important long-period basin-generated surface waves that will occur at the edge of the South Island's large

sedimentary basins and dominate ground motion amplitudes. Observations of very strong long-period motions from the  $M_w$  9.0 Tohoku earthquake in Tokyo (Takewaki et al. 2011) (distance 120 km) and directivity–basin coupling in simulated ground motions in Los Angeles due to future major earthquakes on the southern San Andreas fault (Olsen 2000; Graves et al. 2011a) (distance 45 km) both illustrate the importance of basin-generated surface waves and near-surface site response, phenomena which can only be modelled via advanced physics-based simulation methods (Graves et al. 2011b; Bradley 2012; Graves & Pitarka 2015; Olsen & Takedatsu 2015).

The observed ground motions in the 2010–2011 Canterbury earthquakes (e.g. Bradley & Cubrinovski 2011; Bradley 2012) have also highlighted the importance of directivity, basin-generated surface waves and surficial site effects in a New Zealand context. Systematic biases of empirical ground motion prediction models relative to observations at specific locations have been identified (Bradley 2015), and the use of physics-based ground motion simulations (Bradley et al. 2015a, 2015b; Lee et al. 2015) have provided a causative explanation for these observations and demonstrated the fidelity of such simulations, both for forensic analysis of historical earthquakes and also for prediction of future earthquake scenarios.

In the above context, this paper provides the first high-fidelity modelling of the severity of ground motions in the South Island region from future major earthquakes on the Alpine Fault using three-dimensional (3D) numerical simulations, in particular, examining the effect of hypocentre location and comparing with conventional empirical ground motion prediction estimates. The following sections provide a discussion on the Alpine Fault rupture scenarios and the 3D crustal model of the South Island considered, the simulated ground motion intensity over the South Island, comparisons with ground motion estimates from conventional empirical models and derived Modified Mercalli Intensity (MMI) values for regional risk and impact assessments. Discussion is also given to the use of the simulations by the South Island Civil Defence Emergency Management (CDEM) 'Project AF8' (Alpine Fault Magnitude 8) exercise.

## 2. Rupture scenarios investigated

### 2.1. Rupture geometry

Figure 1 illustrates the mapped faults in the South Island. Attention here is restricted to the Alpine Fiord-to-Kelly (AlpineF2K) segment of the Alpine Fault, as documented in Stirling et al. (2012). While being a characteristic segment in the model of Stirling et al. (2012), it is recognised that such segment boundaries are a modelling assumption, and further research is needed to understand the potential for other rupture extents, and the use of seismic hazard methods which can be used to determine corresponding event rates

(e.g. Field & Page 2011). As a result, the AlpineF2K rupture geometry represents a compromise between a catastrophic, but relatively unlikely, earthquake which runs the full length of the island (i.e. from the offshore section of the southern end of the South Island to the northern end of the Marlborough fault zone or beyond) and an earthquake on smaller segment of the Alpine Fault.

Figure 1 illustrates the surface projection of the AlpineF2K segment, with a geometry of 411 km along strike, with a dip of 60 degrees. In Stirling et al. (2012), the maximum seismogenic depth is considered as 12 km, based on background seismicity. However, research also indicates rupture beyond the seismogenic depth into the ductile crust is likely in major earthquakes as a result of kinematic considerations (e.g. King & Wesnousky 2007) and may not be illuminated by aftershocks. The uncertainty in rupture width is a significant component of uncertainty in inferred rupture areas in past earthquakes and consequently magnitude-area scaling relationships. In this context, Graves and Pitarka (2015, and references therein), identify that ignoring this results in a concentration of slip at shallower depths and modelled long-period ground motions that are inconsistent with observations. Graves & Pitarka (2015) thus recommend the consideration of rupture below the seismogenic depth with a tapering of the rupture velocity, rise time and corner frequency, which we consider over the depth range of 12–15 km. Clearly, variations in the fault segment geometry and uncertainty in the rupture depth will affect the resulting simulated ground motions, and should be considered in future studies.

### 2.2. Rupture kinematics

The Alpine Fault is recognised as a predominantly right-lateral strike-slip fault, with a component of reverse motion. Stirling et al. (2012) adopted a magnitude of  $M_W 8.1$  for the AlpineF2K geometry based on the magnitude-area scaling relationship of Hanks & Bakun (2002) (with a maximum depth of 12 km leading to a down-dip width of 13.9 km). For large events there is significant variability in magnitude-area scaling relationships. When used with empirical ground motion models (as was the purpose of the magnitudes estimated in Stirling et al. 2012), the effects of magnitude uncertainty are not overly significant as empirical models have a built-in magnitude-area relation which results in empirically estimated long-period amplitudes effectively scaling with  $M_O^{1/3}$  (Graves et al. 2011b). In contrast, simulated long-period ground motions from physics-based methods scale nearly linearly with  $M_O$ . As a result, it is critical that consistent fault areas and magnitudes are assigned. When faced with the same issues, Graves et al. (2011b) and Graves & Pitarka (2015) express the opinion that the model of Leonard

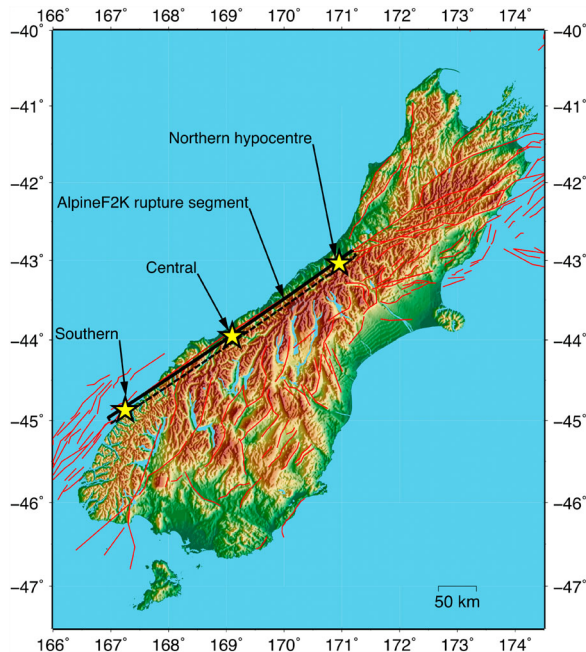


**Figure 1.** Mapped faults in the South Island of New Zealand (Stirling et al. 2012), including the modelled 411 km-long Alpine Fiord-to-Kelly (AlpineF2K) segment and the three hypocentre locations considered.

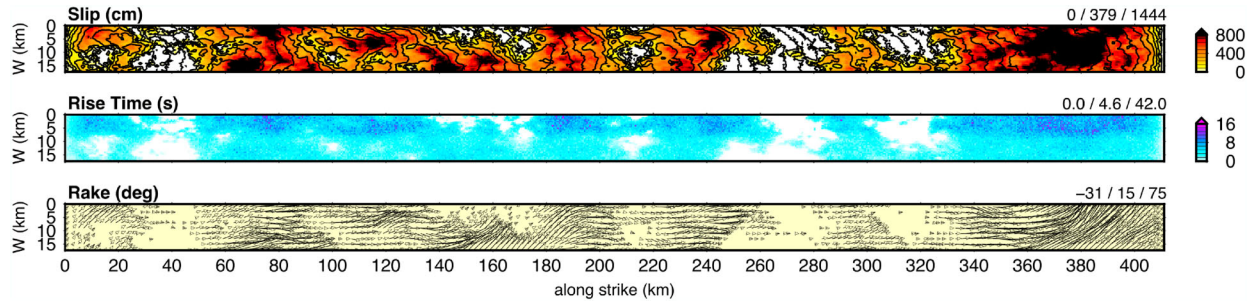


**Figure 2.** Illustration of the slip amplitude, rise time and rake direction of the  $M_w 7.9$  AlpineF2K kinematic rupture considered with a Southern hypocentre. The numbers in the top right of each figure panel represent the minimum/mean/maximun of the quantity depicted.

(2010) is both most consistent with the inferred depth extent of large ruptures (see discussion in previous section) and also provides the best validation results for simulations compared with past earthquakes. As a result, we adopted the scaling relation of Leonard (2010) which resulted in a  $M_w 7.9$  rupture for the fault geometry considered (maximum depth of 15 km). The effect of uncertainty in magnitude for this fault geometry on the resulting simulated ground motion amplitudes is a topic for future research.

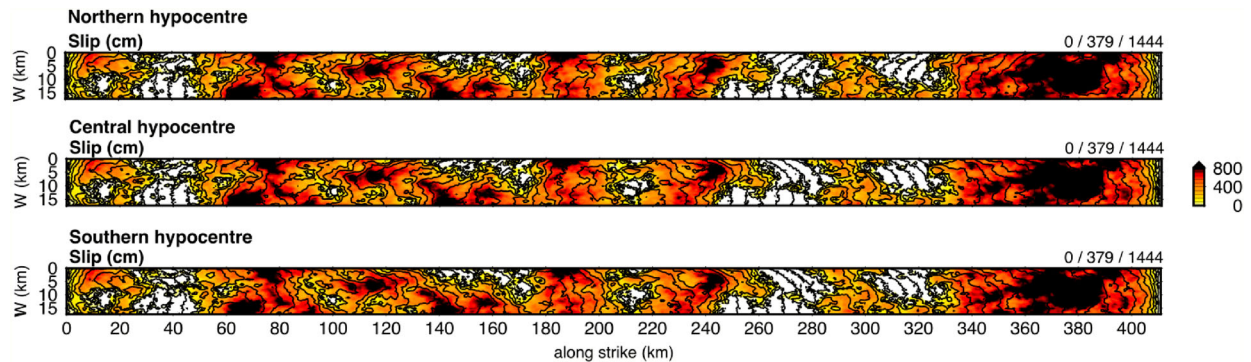
Finally, an average rake of  $\lambda = 15$  degrees was considered, given the predominant right-lateral strike-slip deformation (simulations suggest reasonable variations in the average rake about this adopted value have little effect on ground motion amplitudes)

Figure 2 illustrates the slip amplitude, rise time and rake direction variation of rupture across the fault surface for rupture with a southern hypocentre. In the slip amplitude portion of the figure (top panel), contours indicate the temporal evolution of rupture. It is important to note the significant variation in the slip amplitude, rise time and rake of the rupture, which are quantified in the top-right of each figure panel via minimum/mean/maximun values. Such large variations in rupture properties are both observed from source inversion studies and also necessary to provide a sufficiently incoherent rupture, and resulting

wavefield, to provide ground motion amplitudes consistent with observations (Graves & Pitarka 2015).

For large magnitude earthquakes the hypocentre location may strongly effect the resulting ground motion amplitudes over the South Island as a result of directivity and basin-generated surface waves. As a result, three different hypocentral locations were considered for the AlpineF2K source, as illustrated in Figure 1, which are herein referred to by their relative locations as ‘Southern’, ‘Central’, and ‘Northern’ hypocentres. It is noted that following research indicating that the effect of stochastic slip variability on ground motion amplitudes is small relative to variability in the assumed hypocentre location (Razafindrakoto et al. 2016), multiple realisations of the stochastic slip distributions were not considered due to limitations in high-performance-computing allocation size (although they should be in a more rigorous assessment).

An illustration of the stochastically generated slip distribution models for each of the three hypocentre locations is shown in Figure 3. As noted, because emphasis was placed on the effect of hypocentre location (i.e. rupture propagation direction), the same stochastic perturbation of the slip distribution was used in the Graves & Pitarka (2015) rupture generator. As a result, the gross features of the slip amplitude shown by the colour scale in Figure 3 are similar in



**Figure 3.** Illustration of the three slip distributions over the AlpineF2K fault plane for the Southern, Central and Northern hypocentre rupture scenarios. The gross features of the slip amplitudes are similar among all three, however, because of the difference in hypocentre location, the effect of rupture propagation and coupling of stochastic perturbations in slip amplitude and local rupture velocity leads to small scale variations.

all three rupture cases. However, because of the different hypocentre locations, and also the correlation between slip amplitude and local rupture propagation velocity, the small scale variations are different, as well as the absolute rupture initiation time of each segment being substantially different. The distributions of rise time and rake direction are only correlated to the perturbation of the slip amplitude, and therefore are the same for all three ruptures and thus not repeated here.

### 3. 3D crustal model of the South Island

Figure 4 provides an illustration of the South Island velocity model (SIVM) (Bradley et al. 2015b; Lee et al. 2015; Thomson et al. 2016), which describes the adopted 3D model of the crust in the region for seismic wave propagation. Two sets of transects are provided in this Figure, as shown in the inset panel. The first of these are transects over the wider South Island region, in particular, through the alpine region. The second of these are through the Canterbury region. It can be seen that the Canterbury region contains explicit high-spatial-resolution modelling of the sedimentary basin deposits, as discussed in detail by Bradley et al. (2015b) and Lee et al. (2015), which is not present

over the wider South Island region. High-resolution sedimentary basin models are critical for accurate and precise modelling of ground motion amplitudes at frequencies of engineering interest ( $f=0\text{--}25\text{ Hz}$ ), but their development is non-trivial and not currently available outside of Canterbury. As a result, the subsequently presented ground motion amplitudes from AlpineF2K ruptures can be considered most realistic in the Canterbury region, while on-going work is developing basin-specific models for other South Island sedimentary basins to enable improved simulation predictions in future.

Ground motion simulation results utilising the SIVM have been validated against observations for earthquake events in the 2010–2011 Canterbury earthquake sequence (Razafindrakoto et al. 2015), as well as small magnitude events in the Canterbury foothills (Nazer et al. 2016).

### 4. Simulated ground motion intensities

#### 4.1. Simulation methodology and computational details

Ground motion simulation was undertaken using the Graves & Pitarka (2015) methodology, a ‘hybrid’ approach in which the low frequency waveforms are

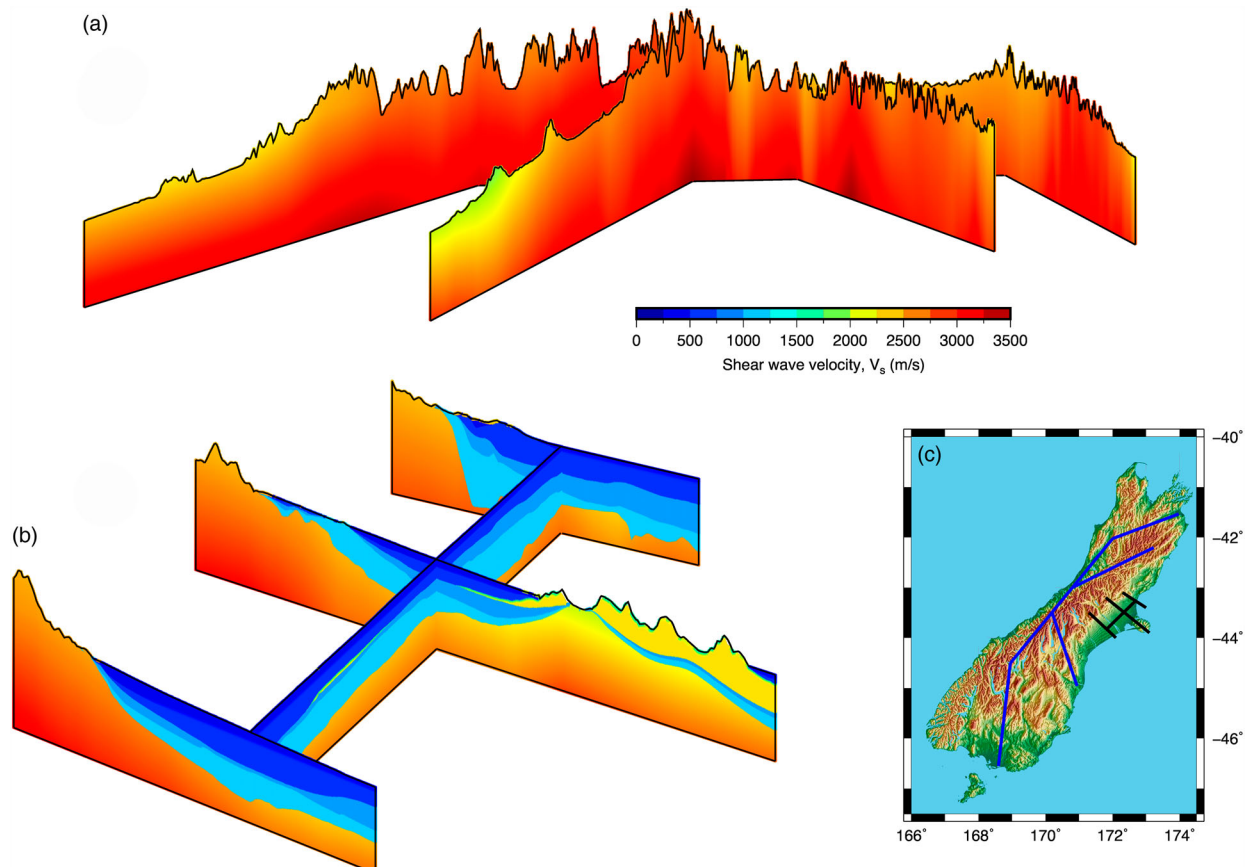


**Figure 4.** (a and b), Transects of the South Island Velocity Model (SIVM) (Bradley et al. 2015b; Lee et al. 2015; Thomson et al. 2016), illustrating the modelled variation of seismic velocity over the South Island used in the ground motion simulations. The location of the transects are identified in (c). Note the explicit high-resolution modelling of the sedimentary basin in the Canterbury region in B.

comprehensively computed by solving the elastodynamic equation in the 3D crustal model domain, while the high frequency waveforms utilise a phenomenological simplified physics approach. Because we focus on the resulting peak ground velocities (PGVs) of ground motion in subsequent sections, and these are largely the result of low frequency ground motion, attention here is restricted to discussion of the low frequency portion of the simulations.

The ground motion simulations were performed within a computational domain of  $800\text{ km} \times 350\text{ km} \times 100\text{ km}$ , with a finite difference grid spacing of either 0.4 or 0.1 km. It was found that the grid spacing did not appreciably influence the estimated PGV values, and therefore, in the context of the available computational allocation, the majority of simulations, including those shown subsequently, are based on the 0.4 km grid. The cartesian finite difference grid does not model topographic effects, which are not considered important for the frequency band in the low frequency 3D simulation, but should be modelled if such simulations were extended to higher frequencies. In the Canterbury sedimentary basin a minimum shear wave velocity of  $V_s = 500\text{ m/s}$  was considered (yielding maximum frequencies of the low frequency waveforms of 0.25 Hz and 1 Hz, respectively for the two considered computational grids), while outside the Canterbury basin the minimum shear wave velocity is generally greater than  $V_s = 1000\text{ m/s}$  (giving maximum frequencies of 0.5 and 2.0 Hz). Additional computational workflow details are discussed in Bae et al. (2016). A time increment of  $\Delta t = 0.005\text{ s}$  was utilised, resulting in 50,000 time steps to produce simulated ground motions for a target duration of 250 s. The

ground motion simulations were performed on the NeSI ‘Fitzroy’ Power6 cluster (<https://www.nesi.org.nz/services/high-performance-computing/platforms>). For the 0.4 km grid spacing, using 512 compute cores required 2.5–3.0 hours of wall clock compute time, while the 0.1 km grid spacing using 1024 cores required approximately 90 hours of compute time (a longer wall clock time because of checkpointing).

#### 4.2. Effects of rupture directivity and directivity-basin coupling

Figure 5 illustrates three ‘snapshots’ of the ground motion wavefield (in the form of PGV amplitudes) at  $t = 50, 130$  and  $180\text{ s}$  following rupture initiation for the case of a Southern hypocentre rupture. The three snapshots shown in the figure illustrate significant directivity (Somerville et al. 1997) in the wavefield as the rupture propagates from south to north (Figure 5 (a–b)), directivity-basin coupling in the Canterbury region (Graves et al. 2011a) (Figure 5(b–c)) and significant amplitudes in the northern South Island despite the distance from the rupture itself. Video animations of the Southern hypocentre simulation, as well as the Central and Northern hypocentre simulations are available at: <https://www.youtube.com/watch?v=FxiHB0FJF5k>.

#### 4.3. Effect of hypocentre location on PGV amplitudes

Figure 6 illustrates the spatial distribution of PGV resulting from the three different hypocentre locations considered. For all three different rupture models it

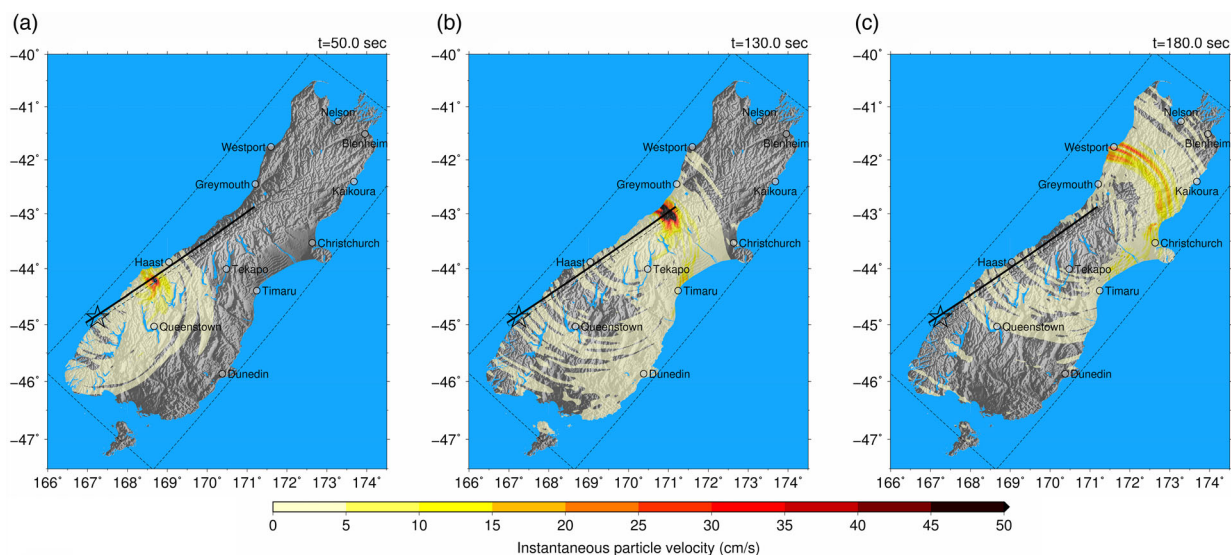


**Figure 5.** Illustration of the particle velocity (vector maximum in the horizontal plane) at three time instants during ground motion simulation of the Southern Hypocentre AlpineF2K rupture scenario: (a)  $t = 50\text{ s}$ , illustrating significant rupture directivity in the wavefield; (b) directivity-basin coupling as the wavefield enters the Canterbury basin; (c) directivity leading to relatively large amplitudes North of the rupture and critical reflections resulting in a long duration of significant ground motion in the Canterbury sedimentary basin.

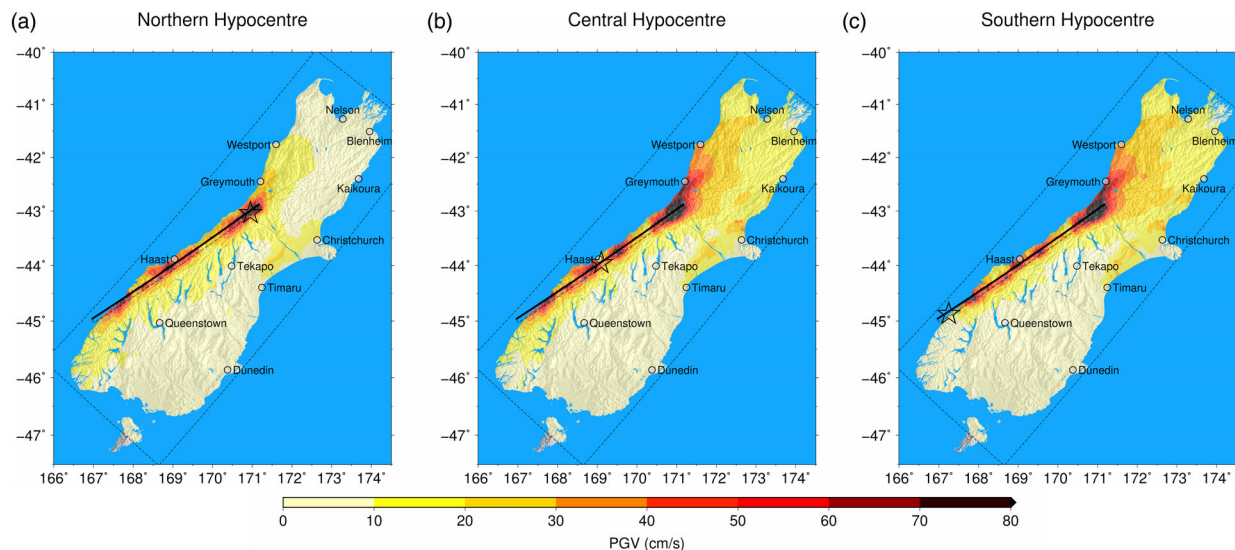


**Figure 6.** Spatial distribution of peak ground velocity (PGV) over the South Island for the three rupture scenarios considered. The effect of hypocentre location on the directivity and directivity–basin coupling is most prominent in the Canterbury region and northern South Island.

can be seen that the intensity of ground motion directly in the near-field of the source rupture is highly variable as a result of the complex variation in slip amplitude, rise time and rupture velocity across the rupture surface (Figure 3). As previously noted, because the same stochastic perturbation was used for the generation of rupture models in all three hypocentres considered, it is important to emphasise that particularly in the near-fault region the consideration of different rupture perturbations would yield a notable difference in the spatial variation of ground motion intensity. Generally speaking, as the distance from the rupture increases, it can be seen that ground motion amplitudes decrease as a result of geometric spreading. However, this general trend is highly variable as a result of the effects of directivity and directivity–basin coupling, which leads to waveguide effects in specific geographical regions.

The difference between the PGV spatial distribution for the three hypocentre locations considered in Figure 6 is explicitly illustrated in Figure 7, via the ratio of PGV from the Northern and Central hypocentre ruptures relative to that of the Southern hypocentre. A discrete colour palette for these figures is used to distinguish differences of approximately 10%, 20%, 50% and a factor of two. It can be seen that a significant variation occurs in the northern half of the South Island, where the results from the Central hypocentre are within 10% (albeit lower) than those from a Southern hypocentre rupture, and yet a Northern hypocentre rupture produces PGV amplitudes that are more than a factor of two lower. A similar trend occurs, although over a smaller geographic region over the southwest of the island (Fiordland and Invercargill), in which the Southern hypocentre simulation produces PGV amplitudes that are more than a factor

of two smaller than those from Central and Northern hypocentres (the two of which produce similar amplitudes in this region). In the central and eastern portions of the southern half of the South Island it can be seen that there is a relatively complex spatial variation in the PGV ratios. In Queenstown it can be seen that the largest amplitude motions occur for the Northern hypocentre scenario, although the ratios indicate that all three hypocentres produce not dissimilar amplitudes. Similarly, in Dunedin, the Northern and Southern hypocentres yield similar PGV amplitudes, both of which are larger than that resulting from a Central rupture initiation. In the Canterbury basin, where a detailed sedimentary model exists (Figure 4), it can be seen that the PGV ratios vary over short spatial distances. In the urban Christchurch region the strongest shaking occurs from the Southern hypocentre scenario; however, in localised areas in the north and southwest of the basin, the Northern and Central hypocentres produce larger amplitudes. In north Westland, the largest amplitudes result from the Southern and Central hypocentres, while in central Westland the amplitudes vary over short spatial distances as a result of the spatial–temporal evolution of rupture in the near-field (which, as noted, will vary for other rupture perturbations).

#### 4.4. Comparison with empirical ground motion estimates

Figure 8 provides an alternative estimate of PGV from AlpineF2K ruptures via a conventional empirical ground motion model (specifically, the median PGV from Chiou & Youngs 2008). The empirical model accounts for the general decay in PGV with source-to-site distance,  $R_{\text{rup}}$ , using simple geometric spreading

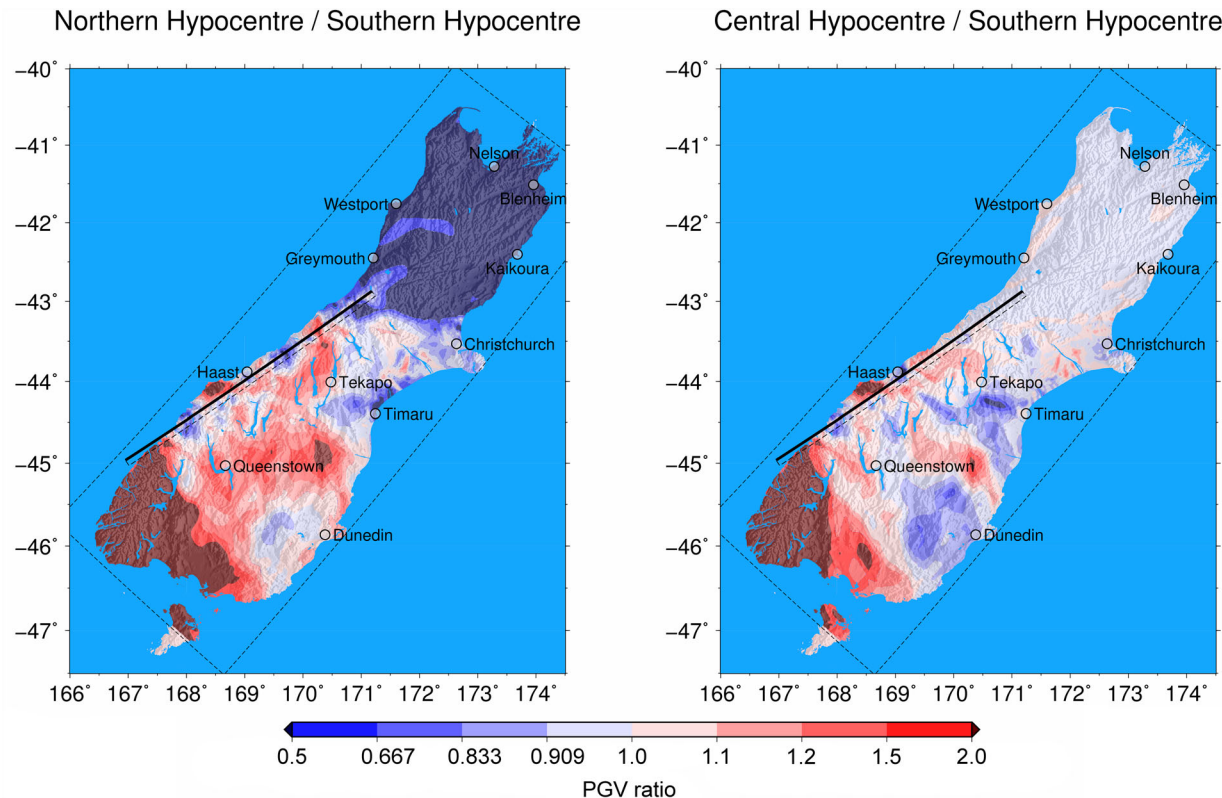


**Figure 7.** Ratios of PGV from the Northern and Central hypocentre simulations relative to that of the Southern hypocentre. The Southern hypocentre simulation produces relatively low amplitudes in Fiordland and Invercargill, while the Northern hypocentre produces relatively low amplitudes in the northern half of the South Island.

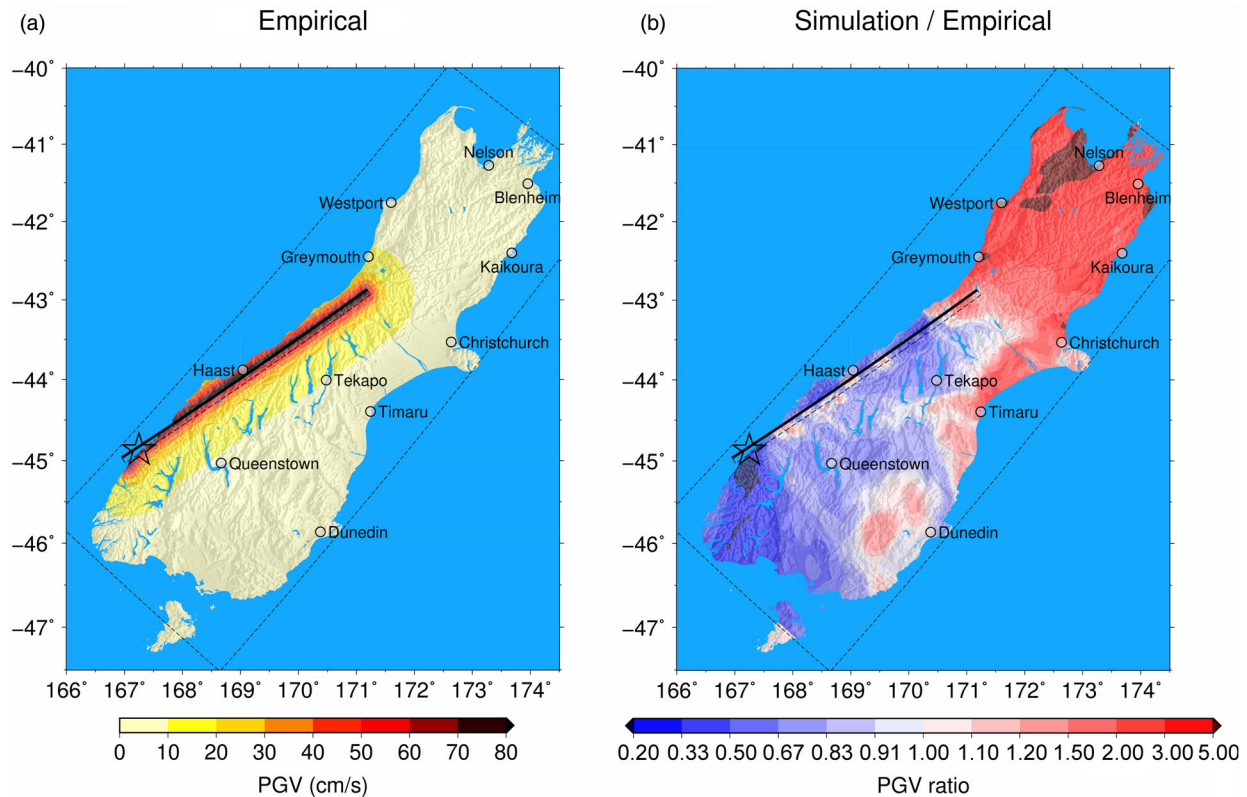
and anelastic attenuation functions (as is evident in Figure 8(a)), and importantly does not explicitly model directivity or directivity–basin coupling.

Figure 8(b) illustrates the ratio of the PGV values from the Southern hypocentre simulation (Figure 6(c)) and the empirical prediction (Figure 8(a)). The warm colours indicate regions in which the simulated intensity exceeds that of the (median) empirical prediction, while cool colours indicate the opposite. Several of the sentiments that we echoed in discussion of Figure 7 are also evident in the examination of Figure 8(b). It can be seen that the empirical model provides larger intensities in the central portion of the southern South Island (e.g. Tekapo, Queenstown) and particularly in Fiordland. This is consistent with the comments in relation to Figure 7 that the Northern hypocentre simulation scenario provides notably greater amplitudes than that of the Southern hypocentre scenario. In the east of the southern South Island it can be seen that the amplitudes of the simulation and empirical predictions are similar for Dunedin, while the simulation is slightly larger for Timaru. In Canterbury, the Southern hypocentre simulation produces PGV amplitudes that are 1.5–3.0 times greater than the empirical prediction (larger values near the significant basin edges in southwest and north east Canterbury, smaller values in central Canterbury and urban Christchurch).

Finally, in the northern half of the South Island it can be seen that the Southern hypocentre simulation produces significantly larger amplitudes than the empirical model. This can be explained as a result of the significant effect of forward directivity (as shown in Figure 5(c)), which is neglected in the empirical model.

#### 4.5. Modified Mercalli Intensity estimates

While PGV provides a useful metric to assess the overall intensity of Alpine Fault ground motions, particularly at moderate-to-large source-to-site distances where the ground motion is dominated by long-period motion, other metrics are useful and necessary for regional impact studies. MMI provides one such alternative measure of shaking, which is particularly utilised for impact assessments to residential housing and other assets which have empirical fragility functions based on historical New Zealand earthquake observations. Figure 9(a–c) illustrates the predicted MMI values, based on the MMI-to-PGV correlation of Worden et al. (2012) for the three hypocentre locations considered. Since there is a one-to-one correlation between PGV and MMI from the correlation of Worden et al. (2012), then the relative trends between the simulated MMI values in Figure 9(a–c) are the same as those discussed with reference to



**Figure 8.** (a) Empirical prediction of median PGV based on Chiou & Youngs (2008); (b) ratio of PGV values between the ground motion simulation for a Southern hypocentre and the empirical PGV estimate in A.

Figures 6 and 7. Given the acknowledged dependence on hypocentre location, Figure 9(d) provides the maximum MMI obtained from any one of the three hypocentre scenario simulations. Based on Figure 9(d), it can be seen that strong shaking (MMI 5+) can be expected over the entire island (east Otago being the exception): over 50% of the South Island experiences very strong shaking (MMI 6+); approximately 20% area experiences severe shaking (MMI 7+); and violent and severe shaking (MMI 9, 10+) occurs in the immediate vicinity of the rupturing segment of the fault.

## 5. Discussion and conclusions

This paper has examined simulated ground motions from major Alpine Fault ruptures. Particular attention was given to the use of advanced ground motion simulation methodologies and modelling of the causative fault rupture and the 3D crustal model of the South Island. The effect of hypocentre location was examined and seen to have a significant effect on ground motion intensity in Fiordland and the northern half of the South Island, as well as more subtle effects in the central and eastern parts of the island. The simulated PGV ground motion intensities were compared with empirical models and also MMI values were computed to provide a simple overview of the island-wide intensity of shaking.

The damage observed in the 2010–2011 Canterbury earthquake sequence (e.g. Cubrinovski et al. 2011; Giorgio et al. 2011; Kam et al. 2011; Bradley et al. 2014), provides a recent illustration of the vulnerability of New Zealand communities to earthquake hazards and the need for further preparation for future earthquakes. A large Alpine Fault earthquake rupture provides a useful scenario for disaster preparedness because of its likelihood of occurrence, expected impact and also far-reaching public awareness. Recognising the above factors, South Island CDEM groups initiated Project AF8, supported by Ministry of CDEM's National Resilience Fund (<http://projectaf8.co.nz/>). The ground motion simulation research summarised in this paper has been utilised by Project AF8, as one possible model for the ground shaking.

Prior Alpine Fault impact assessment studies (Robinson & Davies 2013; Robinson et al. 2016) have been based on ground motion estimates from empirical models. As illustrated in Figures 8 and 9, the ground motion estimates from the presented simulation models suggest greater amplitudes in several notable areas (namely Canterbury and the northern half of the South Island), compared to the previously utilised empirical predictions. Future rigorous assessments should examine more exhaustively the importance of uncertainties in rupture slip perturbations, geometry and 3D crustal models and the overall simulation methodology adopted.

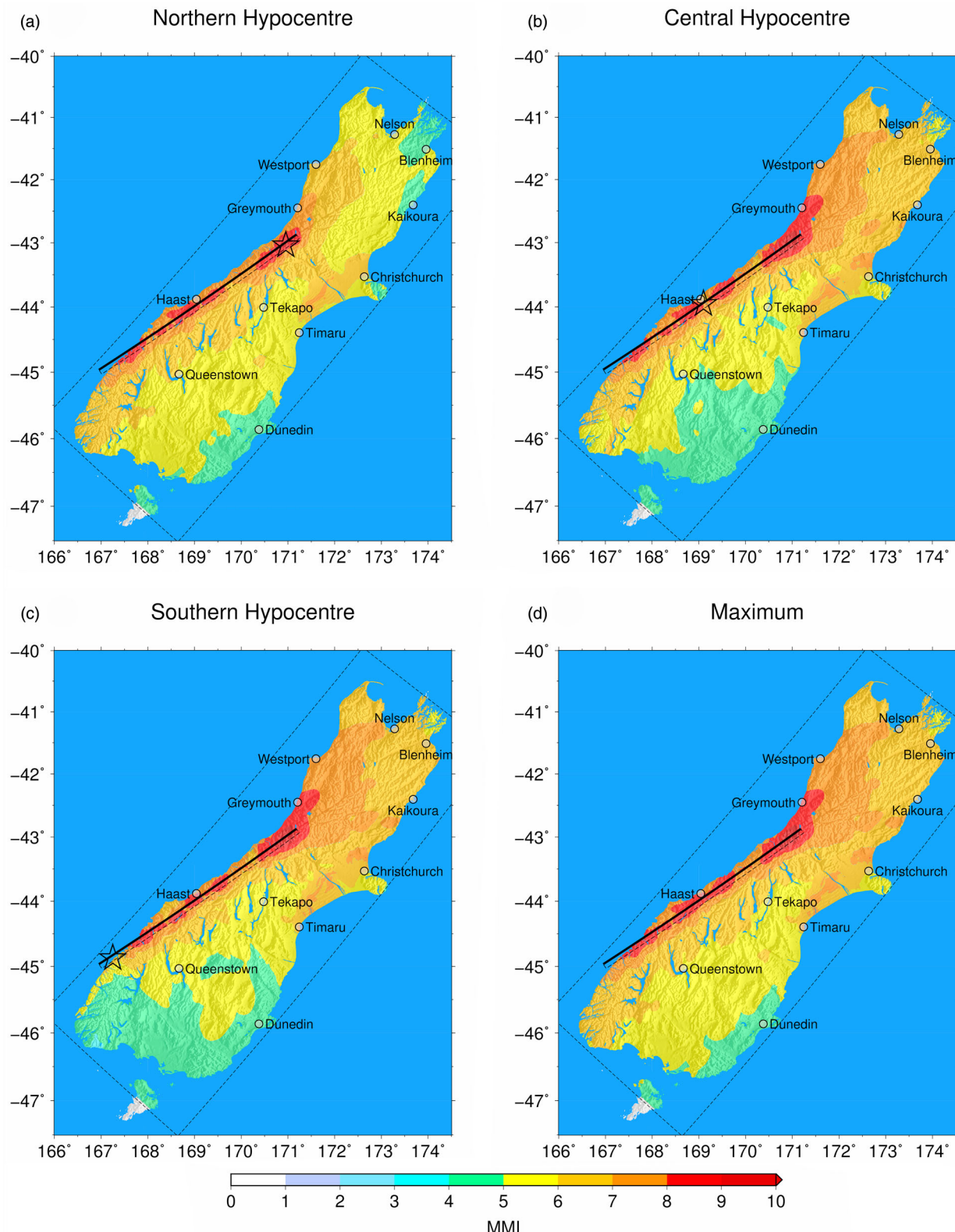


**Figure 9.** Estimated Modified Mercalli Intensity (MMI) over the South Island based on the PGV–MMI correlation of Worden et al. (2012) for: (a) Northern; (b) Central; (c) Southern hypocentres; (d) the maximum MMI over the South Island from the three hypocentre scenarios.

Of course, adequate validation of both empirical and physics-based ground motion simulations are needed to understand their respective predictive capabilities. For the simulation-based predictions in particular, we consider that additional validation efforts already underway, but yet to be completed, will provide greater

confidence in the larger ground motion intensity values that our simulations identify compared to those from empirical predictions. Observations of strong long-period ground motions in Tokyo from the  $M_w 9.0$  Tohoku earthquake and simulated ground motions in Los Angeles from future major southern San Andreas

ruptures illustrate the same directivity and basin-generated waves that are evident in the simulations presented here.

## Data and resources

Ground motion simulations were performed on the National eScience Infrastructure (NeSI) ‘Fitzroy’ Power6 cluster. The South Island seismic velocity model (Bradley et al. 2015b; Lee et al. 2015; Thomson et al. 2016) source code is available at: <https://github.com/ucgmsim/Velocity-Model>. The rupture generator was that of Graves & Pitarka (2015). The adopted QuakeCoRE ground motion simulation workflow is available on GitHub (Bae et al. 2016). Empirical ground motion calculations were performed using OpenSHA (Field et al. 2005). Plotting was performed using GMT <http://gmt.soest.hawaii.edu/>.

## Acknowledgments

The authors thank Caroline Orchison and John Mitchell for their leadership in Project AF8. The high performance computing used in this research was provided through a NeSI merit allocation. This work was also supported by a Royal Society of New Zealand Rutherford Discovery Fellowship and QuakeCoRE: The Centre for Earthquake Resilience. This is QuakeCoRE publication number 0052. Associate Editor: Professor Tim Little.

## Disclosure statement

No potential conflict of interest was reported by the authors.

## References

- Bae S, Polak V, Clare R, Bradley BA, Razafindrakoto HNT. 2016. QuakeCoRE ground motion simulation computational workflow. Paper presented at: QuakeCoRE Annual Meeting, Wairakei, New Zealand.
- Barnes PM, Bostock HC, Neil HL, Strachan LJ, Gosling M. 2013. A 2300-year paleoearthquake record of the Southern Alpine Fault and Fiordland Subduction Zone, New Zealand, based on stacked turbidites. *Bulletin of the Seismological Society of America*. 103:2424–2446.
- Berryman K, Cochran UA, Clark KJ, Biasi GP, Langridge RM, Villamor P. 2012a. Major earthquakes occur regularly on an isolated plate boundary fault. *Science*. 336:1690–1693.
- Berryman K, Cooper A, Norris R, Villamor P, Sutherland R, Wright T, Schermer E, Langridge R, Biasi G. 2012b. Late holocene rupture history of the Alpine Fault in South Westland, New Zealand. *Bulletin of the Seismological Society of America*. 102:620–638.
- Bradley BA. 2012. Ground motion comparison of the 2011 Tohoku, Japan and 2010-2011 Canterbury earthquakes: implications for large events in New Zealand. In: New Zealand Society of Earthquake Engineering Annual Conference, Christchurch, New Zealand; p. 8.
- Bradley BA. 2015. Systematic ground motion observations in the Canterbury earthquakes and region-specific non-ergodic empirical ground motion modeling. *Earthquake Spectra*. 31:1735–1761.
- Bradley BA, Cubrinovski M. 2011. Near-source strong ground motions observed in the 22 February 2011 Christchurch earthquake. *Seismological Research Letters*. 82:853–865.
- Bradley BA, Jeong S, Razafindrakoto HNT. 2015a. Strong ground motions from the 2010–2011 Canterbury earthquakes and the predictive capability of empirical and physics-based simulation models. In: 10th Pacific Conference on Earthquake Engineering, Sydney, Australia; p. 16.
- Bradley BA, Lee RL, Thomson EM, Ghisetti F, McGann CR, Pettinga JR, Hughes M. 2015b. 3D Canterbury Velocity Model (CantVM) – Version 1.0. In: Southern California Earthquake Centre (SCEC) Annual Meeting, Palm Springs, CA.
- Bradley BA, Quigley MC, Van Dissen RJ, Litchfield NJ. 2014. Ground motion and seismic source aspects of the Canterbury earthquake sequence. *Earthquake Spectra*. 30:1–15.
- Chiou B, Youngs R. 2008. NGA model for average horizontal component of peak ground motion and response spectra. Pacific Earthquake Engineering Research Center.
- Cubrinovski M, Bradley BA, Wotherspoon L, Green RA, Bray J, Wood C, Pender M, Allen CR, Bradshaw A, Rix G, et al. 2011. Geotechnical aspects of the 22 February 2011 Christchurch earthquake. *Bulletin of the New Zealand Society for Earthquake Engineering*. 44:205–226.
- Field E, Gupta N, Gupta V, Blanpied M, Maechling P, Jordan T. 2005. Hazard calculations for the Wgcep-2002 forecast using opensha and distributed object technologies. *Seismological Research Letters*. 76:161–167.
- Field EH, Page MT. 2011. Estimating earthquake-rupture rates on a fault or fault system. *Bulletin of the Seismological Society of America*. 101:79–92.
- Ghisetti FC, Barnes PM, Sibson RH. 2014. Deformation of the top basement unconformity west of the Alpine Fault (South Island, New Zealand): seismotectonic implications. *New Zealand Journal of Geology and Geophysics*. 57:271–294.
- Giovinazzi S, Wilson T, Davis C, Bristow D, Gallagher M, Schofield A, Villemure M, Eidinger J, Tang A. 2011. Lifelines performance and management following the 22 February 2011 Christchurch earthquake, New Zealand: highlights of resilience. *Bulletin of the New Zealand Society for Earthquake Engineering*. 44:402–417.
- Graves R, Aagaard BT, Hudnut KW. 2011a. The shakeout earthquake source and ground motion simulations. *Earthquake Spectra*. 27:273–291.
- Graves R, Jordan T, Callaghan S, Deelman E, Field E, Juve G, Kesselman C, Maechling P, Mehta G, Milner K, et al. 2011b. CyberShake: a physics-based seismic hazard model for Southern California. *Pure and Applied Geophysics*. 168:367–381.
- Graves R, Pitarka A. 2015. Refinements to the Graves and Pitarka (2010) broadband ground-motion simulation method. *Seismological Research Letters*. 86:75–80.
- Hanks T, Bakun W. 2002. A bilinear source-scaling model for m-log a observations of continental earthquakes. *Bulletin of the Seismological Society of America*. 92:1841–1846.
- Holden C, Zhao J. 2011. Preliminary broadband modelling of an alpine fault earthquake in Christchurch. *GNS Science Report* 2011/28.
- Kam W, Pampanin S, Elwood K. 2011. Seismic performance of reinforced concrete buildings in the 22 February Christchurch (Lyttelton) earthquake. *Bulletin of the New Zealand Society for Earthquake Engineering*. 44:239–278.

- King GCP, Wesnousky SG. 2007. Scaling of fault parameters for continental strike-slip earthquakes. *Bulletin of the Seismological Society of America*. 97:1833–1840.
- Lee RL, Bradley BA, Ghisetti F, Thomson EM, Pettinga JR, Hughes MW. 2015. A geology-based 3D seismic velocity model of Canterbury, New Zealand. In: New Zealand Society for Earthquake Engineering (NZSEE) Annual Conference, Rotorua; p. 8.
- Leonard M. 2010. Earthquake fault scaling: self-consistent relating of rupture length, width, average displacement, and moment release. *Bulletin of the Seismological Society of America*. 100:1971–1988.
- Nazer M, Razafindrakoto HNT, Bradley BA. 2016. Hybrid broadband ground motion simulations of porters pass earthquakes. In: QuakeCoRE Annual Meeting, Wairakei, New Zealand.
- Olsen K. 2000. Site amplification in the Los Angeles basin from three-dimensional modelling of ground motions. *Bulletin of the Seismological Society of America*. 90: S77–S94.
- Olsen K, Takedatsu R. 2015. The SDSU broadband ground-motion generation module bbtoolbox version 1.5. *Seismological Research Letters*. 86:81–88.
- De Pascale G, Langridge R. 2012. New on-fault evidence for a great earthquake in A.D. 1717, central Alpine fault, New Zealand. *Geology*. [Internet]. [cited 2012 Jun 29];4. Available from: <http://geology.gsapubs.org/content/early/2012/06/21/G33363.1.abstract>
- Razafindrakoto HNT, Bradley BA, Graves RW. 2016. Broadband ground motion simulation of the 2010–2011 Canterbury earthquake sequence. In: New Zealand Society for Earthquake Engineering Annual Conference, Christchurch, New Zealand; p. 8.
- Razafindrakoto HNT, Bradley BA, Thomson E, Graves RW. 2015. Hybrid broadband simulations of the 2010–2011 Canterbury earthquakes. In: Southern California Earthquake Centre (SCEC) Annual Meeting, Los Angeles, USA.
- Rhoades D, Van Dissen R. 2003. Estimates of the time-varying hazard of rupture of the Alpine Fault, New Zealand, allowing for uncertainties. *New Zealand Journal of Geology and Geophysics*. 46:479–488.
- Robinson T, Davies T. 2013. Review article: potential geomorphic consequences of a future great (mw=8.0+) Alpine Fault earthquake, South Island, New Zealand. *Natural Hazards and Earth System Sciences*. 13:2279–2299.
- Robinson TR, Davies TRH, Wilson TM, Orchiston C. 2016. Coseismic landsliding estimates for an Alpine Fault earthquake and the consequences for erosion of the Southern Alps, New Zealand. *Geomorphology*. 263:71–86.
- Somerville P, Smith N, Graves R, Abrahamson N. 1997. Modification of empirical strong ground motion attenuation relations to include the amplitude and duration effects of rupture directivity. *Seismological Research Letters*. 68:199–222.
- Stirling M, McVerry G, Gerstenberger M, Litchfield N, Van Dissen R, Berryman K, Barnes P, Wallace L, Villamor P, Langridge R, et al. 2012. National seismic hazard model for New Zealand: 2010 update. *Bulletin of the Seismological Society of America*. 102:1514–1542.
- Sutherland R, Berryman K, Norris R. 2006. Quaternary slip rate and geomorphology of the Alpine fault: implications for kinematics and seismic hazard in southwest New Zealand. *Geological Society of America Bulletin*. 118:464–474.
- Takewaki I, Murakami S, Fujita K, Yoshitomi S, Tsuji M. 2011. The 2011 off the Pacific coast of Tohoku earthquake and response of high-rise buildings under long-period ground motions. *Soil Dynamics and Earthquake Engineering*. 31:1511–1528.
- Thomson EM, Bradley BA, Lee RL. 2016. The South Island velocity model (SIVM) – version 1: computational implementation and integration within the unified community velocity model (UCVM) framework. In: QuakeCoRE Annual Meeting, Wairakei, New Zealand.
- Wallace LM, Beavan J, McCaffrey R, Berryman K, Denys P. 2007. Balancing the plate motion budget in the South Island, New Zealand using GPS, geological and seismological data. *Geophysical Journal International*. 168:332–352.
- Worden CB, Gerstenberger MC, Rhoades DA, Wald DJ. 2012. Probabilistic relationships between ground-motion parameters and modified Mercalli intensity in California. *Bulletin of the Seismological Society of America*. 102:204–221.
- Yetton M. 2000. The probability and consequences of the next Alpine fault earthquake, South Island, New Zealand [PhD Thesis]. Canterbury: University of Canterbury.